Analysis and prediction of surface topography e volution in laser recovery of monocrystalline sili con

Weiqi Huang[1], Sishuo Yang[1], Jianfeng Xu[1], Junfeng Xiao[1#]

1 State Key Laboratory of Intelligent Manufacturing Equipment and Technology, School of Mechanical Science and Engineering, Huazhong University of Science and Technology, Wuhan 430074, P. R. China
Corresponding Author / Email: xiaojf@hust.edu.cn

KEYWORDS: Laser recovery, Monocrystalline silicon, Surface roughness, Surface topography, Prediction model

Surface defects generated during the machining of monocrystalline silicon optical components weakened the performance of optical systems. Recovery of the damage introduced by mechanical machining to optical components was a crucial approach to enhancing the overall performance of optical systems. In this study, a pulsed laser was employed to recover monocrystalline silicon mirrors post single-point diamond ultra-precision cutting. The surface topography evolution of monocrystalline silicon with varying laser fluence was investigated using white-light interferometry, and a predictive model for laser-recovered surface topography was established. The findings indicated that the recovery process could be divided into six regimes according to the evolution of surface topographical characteristics with varying laser fluence: bulge, coalescence, smoothness, groove, ripple, and ablation. When the laser fluence ranged between 16 and 23 J/cm², surface cutting textures were effectively eliminated, reducing surface roughness from 6 nm to 0.7 nm. The predictive model accurately calculated the post-laser-recovered surface topography, exhibiting a Root Mean Square Error of less than 1 nm in alignment with experimental results. Thermal stress, melting, and vaporization were the primary driving forces influencing surface shaping. By employing the predictive model to effectively coordinate these factors and optimize laser parameters, the recovery of monocrystalline silicon from machining damage was achieved.

NOMENCLATURE

LR = laser recovery	λ = wavelength
P = laser power	τ = pulse width
f = frequency	v = scanning velocity
r = radius	d = scanning pitch
ρ = density	η = absorption rate
c_p = specific heat	δ = penetration depth
T_m = melting point	T_0 = initial temperature

1. Introduction

Ultra-smooth silicon lenses and mirrors play a pivotal role in short-wave optics, prominently in high-power lasers [1], hard X-ray systems [2], and lithography [3]. These applications demand a sur face roughness of less than 1 nm rms, extremely low residual stress, a bsence of surface defects or subsurface damage, and an immaculate la ttice structure. Silicon, a typical hard and brittle material, is pron e to develop residual stress, surface defects, and subsurface dam age during machining. For instance, single-point diamond cutting can introduce high-frequency cutting textures on the surface, le ading to light scattering and a reduction in specular reflectivity or transmittance. Furthermore, phase transformation, dislocation, and cracks may also occur in the subsurface, diminishing the en ergy threshold and transmission efficiency of the element. Laser recovery (LR) is an effective method to reduce surface roughnes s and enhance the subsurface quality of workpieces. In this stud y, LR was employed on monocrystalline silicon subsequent to ul tra-precision cutting (Fig. 1(a)). A novel algorithm for laser flue nce, taking into account scanning velocity and interval was intro duced. The characteristics of surface topography at diverse fluen ce levels were analyzed, and the entire LR process was segment ed into six distinct regimes. Furthermore, a mapping relationship between multiple process parameters and recovery outcomes wa s established, and a predictive model for process parameters that yield optimal recovery result was proposed based on derived di mensionless fluence.

2. Theory

2.1 laser fluence modification

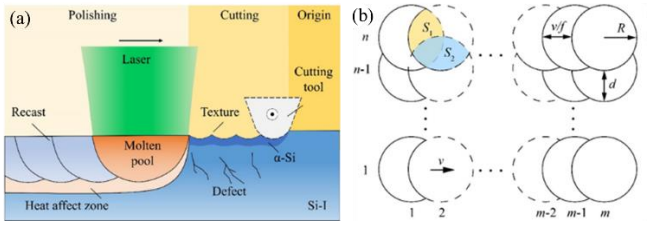

Fig. 1 (a) Principle of laser recovery monocrystalline silicon after ultra-precision cutting, (b) laser scanning strategy.

As far as we could investigate, in the majority of laser applications studies, the commonly used fluence can be expressed as:

$$q_0 = \frac{P}{f\pi r^2} \tag{1}$$

This concise calculation method is convenient when there are fewer variables to consider, as the frequency and radius typically remain unchanged. It describes the fluence deposited by a laser pulse on the workpiece surface. However, in practical processing, the fluence is influenced by multiple parameters. Even with the same power, significant differences in processing effects can be observed under different circumstances, which cannot be explained by Eq. (1). The parameters affecting the fluence can be categorized into two groups: laser parameters, such as wavelength λ, power P, frequency f, pulse width τ, Gaussian beam radius r, and processing parameters, such as scanning velocity v and scanning interval d. In most laser processing applications, a progressive scanning strategy was employed for the recovery process (Fig. 1(b)), and the actual scanning region consisted of a superposition of $m \times n$ laser spots. Therefore, the expression for the laser fluence considering the scanning speed and scanning pitch can be rewritten as

$$q^* = \frac{mnP}{fS} \tag{2}$$

where S is the actual recovery area, which can be calculated as

$$S = 4r^2 + 2(n-1)rd + (m-1)\left[(n-1)d + 2r\right]\frac{v}{f} \tag{3}$$

2.2 Dimensionless Parameter Model

The laser wavelength determines the material's absorption rate (η) and absorption depth (δ). Selecting an appropriate laser wavelength based on material properties, surface conditions, and subsurface conditions is a primary task in laser processing. The laser frequency represents the number of pulse laser interactions with the workpiece surface per second. Higher frequencies result in a denser distribution of melt pools and allow for higher permissible scanning velocities. When the power remains constant, higher frequencies result in lower peak power. Therefore, achieving the same effect as low-frequency lasers typically requires higher power. Pulse width represents the duration of the individual laser pulse's interaction with the workpiece and is usually directly related to the existence time of the melt pool. Rough surfaces require a sufficient duration of melt flow for surface smoothing, but excessively large pulse widths can intensify melt pool convection, leading to the generation of high-frequency structures on the surface due to the Marangoni effect [4]. Scanning velocity and spacing affect the overlap rate of laser spots and need to be matched with the laser frequency. Excessive scanning velocity or spacing can cause discrete deposition of energy, resulting in incomplete workpiece recovery. Conversely, excessive energy deposition and reduced recovery efficiency can occur with too small scanning velocities or spacing. Based on the aforementioned parameters, this study proposes a dimensionless parameter ε to characterize the fluence, expressed as

$$\varepsilon = \frac{Incident\ Energy}{Melting\ Energy} = \frac{E}{H} \tag{4}$$

ε represents the ratio between the incident energy during LR and the energy required for melting in the heat-affected zone. The incident energy and melting energy are denoted as

$$E = mn\eta\hat{P}\tau \tag{5}$$

$$H = V\rho c_p\left(T_m^{\,e} - T_0\right) \tag{6}$$

where $\hat{P} = P/f\tau$ is peak power, represents the energy output of laser during the duration of one pulse width. mn represents the number of scanning pulses. For practical convenience in actual applications, it can be replaced with the dimensions of the scanning area as follows:

$$\begin{aligned} m &= \frac{(L-2r)f}{v} + 1 \\ n &= \frac{(W-2r)}{d} + 1 \end{aligned} \tag{7}$$

where L and W represent the length and width of the recovery area, ρ and c_p denote the density and specific heat capacity of single crystal silicon, $T_m^{\,e} = T_m + L_m/c_p$ is the effective melting point considering latent heat of melting, L_m is the latent heat, T_m is the melting point, and T_0 is the initial temperature [5]. V represents the volume of the laser-affected zone and is calculated as

$$V = S\delta \tag{8}$$

where δ is the laser penetration depth, which is related to the laser wavelength and material optical properties. Substituting Eqs (5), (6), and (8) into Eq. (4) yields:

$$\varepsilon = \frac{mn\eta P}{f\delta S\rho c_p\left(T_m^{\,e} - T_0\right)} \tag{9}$$

It represents a dimensionless fluence that considers most of the laser and processing parameters.

Table I

Overview of LR parameters.

Characteristic	Value
Laser power (W)	0-25
Pulse width (ns)	12.4-37.2
Frequency (kHz)	50-200
Diameter (μm)	60
Velocity (m/s)	0.05-1

3. Fluence-induced surface topography evolution

In order to investigate the role of fluence, we conducted las er scribing experiments by scanning in a single direction along t he *x*-axis. The method of inferring the overall recovery effect ba sed on the morphological features of scribing is reasonable. The results of large-area LR could be considered as the superposition of single point or line recovery [6-7].

A series of surface topography at different laser fluence is s hown in Fig. 2, and the laser parameters is list in Table I. Ther mal stress (Fig. 2(a)), melting (Figs. 2(b)-(e)), and vaporization (Figs. 2(f)-(h)) are identified as the driving forces behind the co nstruction of surface topography. These corresponded to the typi cal surface features of bulge, smoothness, and groove, respective ly. Based on the characteristics of the surface topography, the pr ocess could be further divided into six regimes:

I-Bulge (2.52 J/cm^2 < q^* < 8.19 J/cm^2): The morphology of the cutting texture is essentially preserved. The laser irradiation induced plastic bulges on the surface due to thermal stress, with a height of approximately 7 nm, corresponding to the transitional region.

II-Coalescence (8.19 J/cm^2 < q^* < 10.4 J/cm^2): The original shape of the texture is not maintained, and fractures occurred due to weak melting along the centerline in the scanning direction (*x* axis). The texture exhibited a slight tendency to coalesce longitudinally (*y* axis). As the fluence increased to 8.51 J/cm^2, the cutting texture experienced noticeable melting. As demonstrated in Fig. 2(c), the breakage and coalescence of the texture are clearly visible in the enlarged figure.

III-Smoothness (10.4 J/cm^2 < q^* < 23.78 J/cm^2): During this regime, the molten silicon had sufficient flow time to achieve smoothness. As the fluence increased, the surface pores (marked by circles in Fig. 2(d)) left over from the previous regime are filled, and the melting zone extended in the direction indicated by arrows. The lowest surface roughness is attained in this regime (Fig. 2(e)), and detailed results are presented in Fig. 3.

IV-Groove (23.78 J/cm^2 < q^* < 27.25 J/cm^2): The temperature at the centerline slightly exceeded the boiling point (2628 K). T he recoil pressure generated by the vaporization of molten silico n imparted a downward momentum to the molten pool, resulting in a concave shape and the flow of displaced fluid to both sid es. Subsequently, a grooved structure with a concave middle (va lley) and convex sides is formed upon solidification (Fig. 2(f)).

V-Ripple (27.25 J/cm^2 < q^* < 40.48 J/cm^2): The increased fluen ce extended the existence time and temperature gradient of the molten pool, enhancing the Marangoni flow effect. This led to t he accumulation of materials at the edges of each molten pool, ultimately generating a ripple structure in the valley. The profile of the centerline is depicted in Fig. 2(g), and the period of eac h ripple corresponds to the spacing between pulsed spots.

VI-Ablation (q^* > 40.48 J/cm^2): Intense flow and vaporization occurred, resulting in the formation of stratiform irregular structu res (indicated by black arrows) and punctiform irregular structur es (indicated by white arrows) in the valley. Material accumulati on at the edges is also observed.

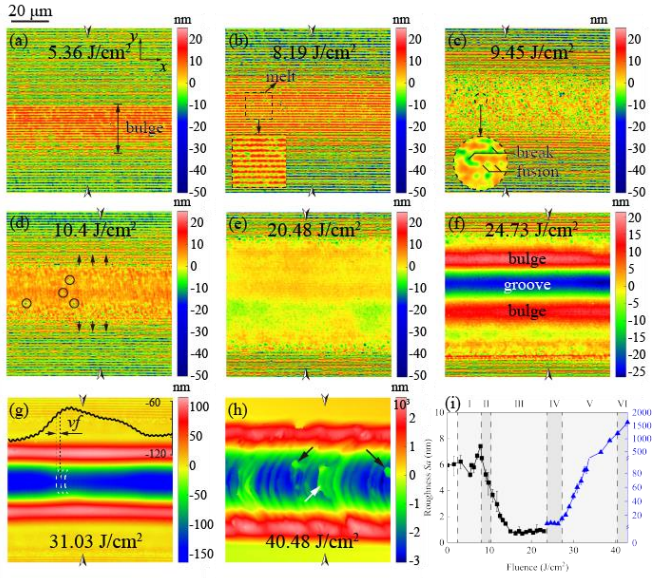

Fig. 2 (a-h) Evolution of Laser scribing topography with fluence, (i) the relationship between surface roughness and fluence.

Figure 2(i) summarized the relationship between surface roughne ss and fluence, with each error bar representing measurements ta ken at five locations. The initial undulation in roughness is attri buted to the inherent fluctuations in the workpiece. In Regime I, the surface roughness gradually increased by approximately 1.5 nm. Following the melting process (Regimes II-III), the roughne ss rapidly decreased until it reaches a stable value of 0.8±0.1 n m. During this period, the melted high-frequency roughness feat ures had sufficient time to flow and flatten, resulting in a rough ness level approximately 90% lower than the initial surface. The stable period represented the optimal window for recovery, with a fluence range of 14.96 - 23 J/cm^2. When the surface topogra phy exhibits the characteristics of vaporization, the roughness ex perienced a significant jump of 12.3 times (8.2 nm). The rough ness of regime VI remained relatively stable at 8.7±0.5 nm until the fluence reached a threshold that induced significant Marang oni flow. In regime V, the roughness started to exhibit exponent ial growth, necessitating the use of an additional longitudinal axi s on the right to depict the roughness of regimes IV-VI on the same graph as regimes I-III. Once the fluence surpassed 42.84 J /cm^2, the roughness exceeded 1600 nm.

4. The prediction model for process parameters

Our research [8] revealed a fundamental correlation between the lowest surface roughness and the optimal subsurface quality. Consequently, a mapping relationship could be developed to determine the optimal LR parameters for various working conditions. The relationship between these parameters and surface roughness is established using the dimensionless fluence introduced in Sec. 2.2. Initially, the dimensionless velocity is defined as follows:

$$v^* = \frac{vL_c}{\alpha} \qquad (10)$$

where L_α represented the characteristic length, defined here as the laser spot displacement within a single pulse.

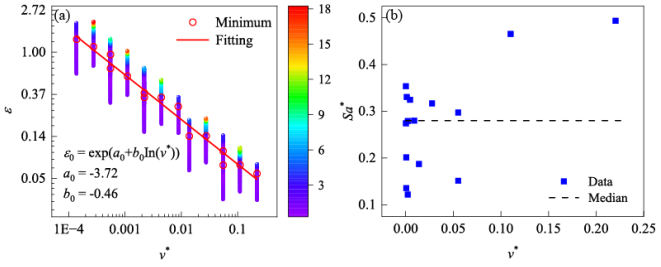

Fig. 3 (a) Prediction model of process parameters corresponding to the minimum relative roughness. (b) Minimum relative roughness corresponding to different v^*.

Based on the experimental results, a predictive model for the minimum surface roughness in LR of single crystal silicon considering multiple parameters is established, as shown in Fig. 3(a). The surface roughness Sa of the silicon wafers used in this study ranged from 3 to 7 nm. To mitigate the influence of roughness variation at different experimental locations on the evaluation of recovery effects, a relative roughness $Sa^* = \overline{Sa} / Sa$ is employed by dividing the post-recovery roughness by the initial roughness. By establishing the mapping relationship between laser parameters, processing parameters, and surface roughness, the minimum relative roughness positions for different v^* values are fitted as

$$\varepsilon_0 = e^{a_0 + b_0 \ln v^*} \tag{24}$$

When the surface roughness is at its minimum, there existed an exponential relationship between v^* and ε (R^2=0.99), with a value of $a_0 = -3.72$, $b_0 = -0.46$. In Regions I-II, where $\varepsilon \le \varepsilon_0$, Sa^* fluctuated around 1 due to plastic expansion or insufficient melting. In region III, ε is distributed near the fitting function, representing the optimal subsurface quality and surface roughness. In Regions IV-VI, where $\varepsilon \ge \varepsilon_0$, the roughness increased due to vaporization and Marangoni convection, resulting in $Sa^* > 1.5$. The relationship between Sa^* and v^* is shown in Fig. 3(b), with Sa^* ranging from 0.12 to 0.5, indicating a reduction in surface roughness by 50% to 88%. Two data points with $Sa^* > 0.4$ are attributed to excessively large v^*, which resulted in incomplete coverage of the workpiece surface during recovery. The median value of the minimum Sa^* is 0.28, corresponding to a 72% reduction in surface roughness.

5. Conclusions

This study demonstrates the effectiveness of LR in mitigating surface and subsurface defects of single crystal silicon. By optimizing laser fluence, a sub-nanometer surface roughness was achieved. Our model categorizes surface topography evolution into six regimes, each associated with specific material structure changes. Key findings include:

Increasing laser fluence leads to distinct topographies (bulge, smoothness, groove), divided into six regimes (Bulge, Coalescence, Smoothness, Groove, Ripple, and Ablation). Plastic expansion of approximately 7 nm occurs during the bulge region, decreasing after melting onset. Optimal surface quality is achieved during the Smoothness regime, reducing roughness from 6 nm to 0.7 nm. Fluence levels exceeding 23.78 J/cm^2 resulted in Marangoni flow and ablation, which should be avoided due to increased roughness. Incorporating commonly used parameters in LR into dimensionless velocity (v^*) and fluence (ε) allows for easy identification of the corresponding recovery regimes. The lowest median relative roughness achieved is 0.28, a 72% reduction. A prediction model incorporating v^* as a variable provides a reference fluence ε_0 for achieving the lowest recovery surface roughness, guiding the ultraprecision manufacturing of single crystal silicon with sub-nanometer ultra-smooth surface.

REFERENCES

1. K. Ni, X. Cheng, B. Huang, S. Liu, J. Shao, Z. Wu, J. Chen and M. Huang, Quantitative Evaluation of Subsurface Damage by Improved Total Internal Reflection Microscopy, Appl. Sci. 9(9) (2019) 1819.

2. C. Xu, X. Peng, J. Liu, H. Hu, T. Lai, Q. Yang and Y. Xiong, A High Efficiency and Precision Smoothing Polishing Method for NiP Coating of Metal Mirror, Micromachines 13(8) (2022) 1171.

3. Y. Dai and X. Peng, Overview of key technologies for optical manufacturing of lithographic projection lens, J. Mech. Eng. 49(17) (2013) 10-18.

4. F. E. Pfefferkorn, N. A. Duffie, X. Li, M. Vadali and C. Ma, Improving surface finish in pulsed laser micro polishing using thermocapillary flow, CIRP Ann. 62(1) (2013) 203-206.

5. M. Beaudhuin, T. Duffar, M. Lemiti and K. Zaidat, One-dimensional model of the equiaxed grain formation in multi-crystalline silicon, J. Cryst. Growth 319(1) (2011) 106-113.

6. Q. Wang, J. D. Morrow, C. Ma, N. A. Duffie and F. E. Pfefferkorn, Surface prediction model for thermocapillary regime pulsed laser micro polishing of metals, J. Manuf. Process. 20(2015) 340-348.

7. S. Marimuthu, A. Triantaphyllou, M. Antar, D. Wimpenny, H. Morton and M. Beard, Laser polishing of selective laser melted components, Int. J. Mach. Tool. Manu. 95(2015) 97-104.

8. Weiqi Huang, Tao Li, Gui Long, Chuangting Lin, Kai Huang, Zhengzheng Ding, Junfeng Xiao, Jianguo Zhang, Jianfeng Xu, Surface topography and subsurface structure evolution in laser micro polishing of monocrystalline silicon, Opt. Laser Technol., 177 (2024) 111068.